***Original Research Article***

# Valorization of corn cobs into activated carbon through chemical activation and evaluation of their methylene blue adsorption performance for contaminated water treatment


## ABSTRACT

1) Please reduce the abstract

Surface water and groundwater are increasingly degraded due to anthropogenic activities. Improving their quality requires efficient and accessible treatment technologies. This study aims to evaluate the methylene blue removal capacity of activated carbons produced from corncob and chemically activated with $H_3PO_4$. The corncob material was pyrolyzed at 400, 500 and 600 °C, and the resulting activated carbons were characterized by FTIR and SEM–EDS to establish the relationship between surface chemistry, elemental composition and textural properties. Methylene blue adsorption was assessed at pH 6.68 using UV–Visible spectrophotometry, and the equilibrium data were fitted to the Langmuir and Freundlich isotherm models. Thermodynamic parameters were also determined over the temperature range of 305.15–334.15 K. The results reveal a specific surface functionalization (P–O–C, P=O/P–O groups, –OH, C=O, C=C functions) and a hierarchical porosity (micro-, meso- and macropores) that enhances both adsorption kinetics and capacity. A $pH_{PZC}$ of 3.4 confirms the strong affinity toward the cationic dye. The sample activated at 500 °C exhibits an exceptionally high adsorption capacity, with a Qmax of 1,250 $mg.g^{-1}$, a surface area of 1,887.45 $m^2.g^{-1}$ and a methylene blue removal efficiency of 98.62%. The adsorption isotherms are better fitted by the Langmuir model, with separation factors $0 < R_L < 1$ indicating favorable adsorption. The Freundlich constant 1/nF ranging from 0.485 to 0.792 also reflects a favorable adsorption process. Thermodynamic analysis shows $\Delta H° = +29.20$ $kJ{\cdot}mol^{-1}$ and $\Delta S° = +110.643$ $J{\cdot}mol^{-1}.K^{-1}$, leading to $\Delta G° < 0$, consistent with an endothermic and spontaneous process dominated by physisorption reinforced by electrostatic and π–π interactions. From a sustainability perspective, this approach valorizes corncob into a high-performance adsorbent and provides a local, reliable, and cost-effective solution for the treatment of contaminated water.



*Keywords: activated carbons; corncob; Fourier transform infrared spectroscopy; specific surface area; organic pollutant; adsorption capacity.*


## 1. INTRODUCTION

Agriculture is a fundamental pillar of food security and economic development in many developing countries. However, it generates substantial quantities of agricultural residues each year, and their inadequate management poses major environmental risks. Among these residues, corncob a widely available by-product of maize threshing is often discarded or openly burned, leading to greenhouse gas emissions and soil degradation. Its conversion into activated carbon (Chyad and al. 2025) represents a sustainable approach to transforming lignocellulosic waste into high-value materials, in line with the principles of circular economy and environmental protection (Bamba and al. 2009).

Activated carbons are characterized by their high specific surface area, well-developed porosity, and the presence of abundant functional groups (hydroxyl, carbonyl, carboxyl, and phosphate groups), which provide strong interaction capacities with a wide range of organic and inorganic pollutants (Yuen et Hameed 2009). Activation with phosphoric acid ($H_3PO_4$) promotes dehydration and aromatic condensation of lignocellulosic components, leading to the formation of stable microporous structures and a high specific surface area (Yorgun et Yıldız 2015). This treatment also generates oxygen- and phosphorus-containing functional groups (P–O, C–O–P) that enhance the surface reactivity toward organic pollutants (Hashemian et al. 2014).

Several studies have demonstrated that agricultural biomasses are effective precursors for producing activated carbons used in water decontamination (Bamba et al. 2009; Hashemian et al. 2014). In one study, Khan and al. (2020) (Khan et al. 2020) valorized petroleum-derived wastes to produce hydrochars capable of adsorbing toxic metal ions. Their results showed that pore morphology and oxygen-containing functional groups play a decisive role in adsorption performance, a principle that is directly applicable to the adsorption of methylene blue onto plant-based activated carbons. Wabaidur et al. ( 2020) reported that oxygenated functional groups and pore-size distribution in carbon-based composites strongly influence the kinetics and adsorption capacity of cationic dyes. Their findings highlight the importance of surface chemistry and electrostatic interactions between active functional groups and organic molecules such as methylene blue. From a theoretical standpoint, ALOthman (2012) demonstrated that pore texture and specific surface area largely determine the adsorption capacity of mesoporous materials. These concepts are directly transferable to activated carbons, where controlling pore size and connectivity enhances adsorption efficiency.

In Burkina Faso, groundwater pollution represents a major environmental concern. The study conducted by Koné ant al. (2009) in the South-West region of the country highlighted the impact of agricultural inputs on groundwater quality. Similarly, Kafando and al. (2025) investigated the quality of borehole and well water in the city of Koudougou, revealing alarming chemical and microbiological contamination linked to anthropogenic pressures and the vulnerability of the aquifer. These findings call for accessible, sustainable, and environmentally friendly treatment solutions.

The production and use of activated carbons derived from corncob, an abundant local resource, therefore appear as an economically viable and environmentally sustainable alternative for the treatment of contaminated water, particularly those containing organic dyes such as methylene blue. This cationic dye, widely used in the textile, paper, and leather industries, is known for its chemical stability and low biodegradability, which make its natural decomposition difficult (Al-Asadi and al. 2025). According to Abid and al. (2025), synthetic dyes exhibit toxic, mutagenic, and carcinogenic properties that may adversely affect aquatic life and human health.

In view of these challenges, it is essential to develop treatment methods that are not only effective but also economically affordable and adapted to local socio-economic conditions. Although numerous studies have reported the effectiveness of activated carbons in the adsorption of methylene blue (Al-Asadi and al. 2025), few have specifically investigated activated carbons derived from corncob chemically activated with phosphoric acid ($H_3PO_4$) for the removal of this dye.

Despite progress in the valorization of agricultural biomass for activated carbon production, there is virtually no in-depth study on the adsorption performance of $H_3PO_4$ activated corncob-based activated carbons for methylene blue removal, particularly in the context of Sahelian countries. This scientific gap fully justifies the present research.

The overall objective of this study is to evaluate the performance of an activated carbon produced from corncob and activated with phosphoric acid for the adsorption of methylene blue, with a view to its potential application in the treatment of contaminated water. This work provides a major scientific contribution by valorizing an underexploited local biomass for the production of activated carbon while offering a comprehensive physicochemical

2) All citation papers should be based on the Author name. Please correct them in the text.

characterization of the material. It also proposes an in-depth evaluation of its methylene blue adsorption performance, enabling a better understanding of the interaction mechanisms between phosphorylated surface functional groups and cationic dyes. Finally, the study highlights the potential of this material as a local, sustainable, and low-cost solution for the treatment of contaminated water.

## 2. 2. MATERIALS AND METHODS

## 2.1. PRODUCTION OF ACTIVATED CARBONS (AC)

### 2.1.1. PREPARATION OF BIOMASS AND IMPREGNATION

3) The sentence is repeated twice time with different type

The biomass was prepared following a standard protocol. The collected corncobs were first cleaned to remove visible impurities (dust, fibers, and organic residues) in order to minimize ash content and fouling. They were then washed with tap water and distilled water to eliminate fine particles and soluble salts that could obstruct the pores. The material was dried at 105 °C for 24 h to reach a constant mass without thermal degradation. After drying, the corncobs were crushed, ground, and sieved using a Retsch AS 300 Control vibrating sieve to obtain a homogeneous particle size (2.5–5 mm), which promotes uniform impregnation and activation. The activating agent used for impregnation was a commercial orthophosphoric acid ($H_3PO_4$) solution, 85.6% w/w (assay), ACS / Reag. Ph. Eur. grade, Buchs (Switzerland). A mass of 10.0 g of corncob was immersed in 75 mL of 2.0 M $H_3PO_4$ for 48 h to ensure diffusion equilibrium and complete impregnation. The impregnated biomass was then dried at 105 °C for 24 h (Memmert UF110 oven) to stabilize the loading of the activating agent prior to carbonization.

### 2.1.2. Carbonization–activation and post-treatment

4) what is this unit min-1 or related to what/whih items? Please clarify it.

An initial mass $m_i$ of impregnated corncob was placed in crucibles and introduced into a Vecstar Furnaces oven. The samples were carbonized at 400, 500, and 600 °C at a heating rate of 20 °C.$min^{-1}$ for 2 h. The resulting materials were then cooled in a desiccator to minimize oxidation and moisture uptake. For each sample, the initial mass mim_imi and final mass $m_f$ were recorded.

5) What do you mean mim_imi?

The activated carbons obtained were washed with ultrapure water until the pH reached values between 6.70 and 7.00 in order to remove phosphate residues and neutralize the surface, and were then filtered using Whatman filter paper. They were dried at 105 °C for 24 h to achieve a constant mass, then ground and sieved. A particle size fraction between 315 and 630 µm was selected to ensure homogeneity in the adsorption experiments and to minimize diffusion resistance.

## 2.2. Physicochemical characterization of the activated carbons

### 2.2.1. Yield after pyrolysis

The pyrolysis yield reflects the mass loss experienced by the biomass during activated carbon production and represents a key quantitative parameter of the process. In this study, it was determined in triplicate for each type of carbon and reported as the average of the three measurements. The yield (Rdt, expressed in %) was calculated from the initial mass $m_i$ of the impregnated sample and the final mass $m_f$ after thermal treatment. The yield (Rdt) was determined using equation (1).

$$\mathrm{Rdt}(\%) = \frac{m_f}{m_i} \times 100 \quad (1)$$

### 2.2.2. Mass loss

Mass loss, also referred to as the degree of activation or burn-off, quantifies the mass reduction occurring during pyrolysis. It is determined using the formula given in equation (2) below:

$$\Delta m(g) = 100 - \left(\frac{m_f}{m_i} \times 100\right) \qquad (2)$$

where $m_i$ represents the initial mass before pyrolysis and $m_f$ the final mass after pyrolysis. For each type of activated carbon (RMA-2M-400, RMA-2M-500, RMA-2M-600), the burn-off was determined in triplicate (n = 3) and reported as the average of the three measurements.

### 2.2.3. Ash content

The ash content was determined according to the method described by (Ahmed et Dhedan 2012) and ( Kouadio et al., 2019). A 0.50 g sample of activated carbon was placed in a crucible and introduced into a muffle furnace set at 650 °C for 2 h. After removal from the furnace, the crucible was cooled to room temperature and weighed. The ash content was determined in triplicate (n = 3) and reported as the average of the three measurements. The ash content C (%) was calculated using equation (3):

$$C\,(\%) = \frac{m_3 - m_2}{m_1} \times 100 \qquad (3)$$

with $m_1$: mass of the charcoal sample used (g); $m_2$ : mass of the empty crucible before calcination (g) ; $m_3$ : mass of the crucible after calcination of the charcoal (g).

### 2.2.4. Moisture content

Porcelain crucibles were placed in a furnace and heated to 1000 °C for 3 h, then cooled in a desiccator. The mass mmm of the crucibles was measured using an analytical precision balance. The crucibles containing the different activated carbon samples of known mass $m_1$ were then placed in an oven at 105 °C for 24 h. After cooling, the mass $m_2$ was recorded, and the moisture content H (%) was determined according to equation (4) :

$$H(\%) = \frac{m_1 - m_2}{m_1 - m} \times 100 \qquad (4)$$

with $m_1$: mass of the crucible containing the activated carbon before calcination (g); $m_2$ : mass of the crucible containing the activated carbon after calcination (g); m : mass of the empty crucible (g).

### 2.2.5. Point of zero charge ($pH_{PZC}$)

The determination of the point of zero charge ($pH_{PZC}$) was based on the method described by (Lopez-Ramon et al. 1999) and adapted by several authors (Melouki et al. 2020; Tchakala et al. 2012; Maazou et al. 2018). The procedure consisted of introducing 20 mL of a 0.1 mol.L$^{-1}$ NaCl solution into 50 mL Erlenmeyer flasks and adjusting the pH to 2, 4, 6, 8, 10, and 12 by adding 0.1 mol.L$^{-1}$ HCl or NaOH. A mass of 0.1 g of adsorbent (activated carbon) was added to each solution. The mixtures were agitated at 350 rpm for 72 h at room temperature, after which the final pH of each solution was measured. Plotting the final pH as a function of the initial pH allowed determination of the $pH_{PZC}$, corresponding to the pH at which the curve intersects the first bisector (final pH = initial pH).

### 2.2.6. Determination of specific surface area

The specific surface area is one of the most important parameters in the characterization of activated carbons. It represents the total surface available for adsorption per unit mass of material. The higher the surface area, the greater the adsorption capacity of the activated

carbon, due to the increased availability of active sites (Daifullah et al. 2004). In the present work, the specific surface area was determined from methylene blue adsorption data. Methylene blue is commonly used as a molecular probe owing to its well-known molecular size and its ability to uniformly cover the internal pore surface of carbon materials (Yap et al. 2025; Ortiz-Anaya et Nishina 2024). The calculation is based on the relationship given in equation (5):

$$S_L = Q_m \times N_A \times S_{BM} \quad (5)$$

$S_L$ : Langmuir specific surface area ($m^2.g^{-1}$) ; $Q_m$: maximum adsorption capacity ($mg.g^{-1}$) ; $N_A$ : Avogadro's number ($6.022 \times 10^{23}$ $mol^{-1}$); $S_{MB}$ : surface area occupied by a methylene blue molecule ($175 \times 10^{-20}$ $m^2$)

This approach makes it possible to estimate the specific surface area accessible to organic molecules in aqueous solution. Although the BET (Brunauer–Emmett–Teller) method based on nitrogen adsorption is considered the reference technique, the methylene blue method provides a simple, rapid, and suitable alternative for laboratories with limited analytical resources (Yap and al. 2025). It yields reliable results that correlate well with the actual adsorption capacity of activated carbon toward organic pollutants. The specific surface area determined by the methylene blue method cannot be directly compared with BET values, but only correlated to them.

#### 2.2.7. Determination of functional groups by FTIR analysis

The chemical components of the activated carbons were characterized using Fourier Transform Infrared (FTIR) spectroscopy. IR spectra were recorded in the wavenumber range of 400–4000 $cm^{-1}$, with a resolution of 4 $cm^{-1}$, using a Shimadzu FTIR-8400S spectrometer at the University of Mons. Solid samples were prepared as pellets by mixing a small amount of each sample with an appropriate quantity of potassium bromide. The mixture was then compressed under a pressure of ten tons. The resulting pellet was subsequently analyzed using the IR spectrophotometer.

#### 2.2.8. Scanning Electron Microscopy (SEM–EDS) analysis

Scanning Electron Microscopy (SEM) coupled with Energy Dispersive X-ray Spectroscopy (EDS) was used to examine the morphology and perform elemental mapping of the different samples. Analyses were carried out using a HITACHI SU8020 electron microscope available at the Materia Nova research center (University of Mons). Prior to observation, the samples were coated with a conductive carbon layer and mounted on specific sample holders, then directly inserted into the analysis chamber for secondary electron imaging (5 kV; 10 µA).

### 2.3. Determination of the adsorption capacity of the activated carbons

The quality of an activated carbon is assessed by its adsorption capacity toward pollutants, a key parameter in water treatment. For this purpose, the adsorption capacity of the activated carbons was determined using methylene blue (MB). In Erlenmeyer flasks, 80 mL of methylene blue solution prepared at different initial concentrations was brought into contact with 0.05 g of activated carbon. The mixtures were placed on a magnetic stirrer and maintained at a constant stirring speed of 350 rpm for 110 minutes to promote optimal mass transfer and ensure the attainment of adsorption equilibrium. In total, seven (07) solutions with initial concentrations ranging from 73.86 $mg.L^{-1}$ to 6 $mg.L^{-1}$ were used for each activated carbon sample (RMA-2M-400, RMA-2M-500, RMA-2M-600).

After agitation, the residual methylene blue concentrations were determined by UV–Visible spectrophotometry at a wavelength of λ = 660 nm, previously identified as the maximum absorption wavelength of the dye. The equilibrium data obtained were used to model the adsorption process using the Langmuir and Freundlich isotherms. These two models allow

6) Before the author mention shaking rate or stirring speed for Hours but here mention as minuets if the minuets should be as minuets not some elsewhere mention Hours and Minuets. All should be same

estimation of the maximum adsorption capacity of the activated carbons examined as well as the nature of methylene blue adsorption on the prepared materials.

### 2.4. Determination of thermodynamic parameters

The thermodynamic parameters ΔH° (enthalpy change), ΔS° (entropy change), and ΔG° (Gibbs free energy change) were determined from adsorption experiments conducted at 305.15 K, 320.15 K, and 334.15 K. These parameters help identify the spontaneity of the adsorption process (ΔG° < 0), determine its thermal nature (ΔH° < 0: exothermic; ΔH° > 0: endothermic), and evaluate the degree of order/disorder at the AC/MB interface via ΔS° (positive value: increase in disorder; negative value: decrease in disorder).

### 2.5. Langmuir model

The Langmuir model assumes a homogeneous surface containing a finite number of equivalent sites, each capable of adsorbing only one molecule, with no lateral interactions between adsorbed molecules; adsorption is therefore limited to a monolayer (Langmuir 1918). The adsorption equilibrium is expressed by the Langmuir equation (6) below:

$$Q_e = Q_{max}\left[\frac{K_L.C_e}{(1+K_L.C_e)}\right] \qquad (6)$$

where

$Q_e$ (mg.g$^{-1}$) is the amount of solute adsorbed at equilibrium; $C_e$ (mg.L$^{-1}$) is the solute concentration in solution at equilibrium; $Q_{max}$ (mg.g$^{-1}$) is the maximum adsorption capacity; $K_L$ (L.g$^{-1}$) is the Langmuir constant related to the affinity of the adsorbent for the adsorbate.

The Langmuir constants $K_L$ and $Q_{max}$ are determined using the linear form of the Langmuir isotherm (equation 7) based on the fitting of the experimental data:

$$\frac{1}{Q_e} = \left[\left(\frac{1}{Q_{max}.K_L}\right)\left(\frac{1}{C_e}\right)+\left(\frac{1}{Q_{max}}\right)\right] \qquad (7)$$

The graphical representation $\frac{1}{Q_e} = f\left(\frac{1}{C_e}\right)$ (Figure 2) yields a straight line with a slope of $\frac{1}{Q_{max}.K_L}$ and an intercept of $\frac{1}{Q_{max}}$.

### 2.6. Freundlich model

The Freundlich isotherm, which is empirical in nature, is based on the assumption that adsorption occurs on a heterogeneous surface composed of sites with different energies. Unlike the Langmuir model, this model assumes the formation of multiple layers of adsorbate molecules on the adsorbent surface (Freundlich 1907). The adsorption equilibrium according to Freundlich is expressed by equation (8) below:

$$Q_e = K_F.C_e^{\frac{1}{n_F}} \qquad (8)$$

where

$Q_e$ is the amount adsorbed at equilibrium (mg.g$^{-1}$) ; $C_e$ is the solute concentration at equilibrium (mg.L$^{-1}$) ; $K_F$ is the Freundlich constant related to adsorption capacity (L.g$^{-1}$) ; $n_F$ indicates the effect of concentration on adsorption capacity and represents the adsorption intensity.

Equation (9) represents the linear form of the Freundlich equation:

$$\ln Q_e = \ln K_F + \frac{1}{n_F}\ln C_e \qquad (9)$$

The graphical representation $\ln Q_e = f(\ln C_e)$ (Figure 3) yields a straight line with a slope of $\frac{1}{n_F}$ and an intercept of $\ln K_F$.

## 3. RESULTS AND DISCUSSION

### 3.1. Pyrolysis yield and mass loss (burn-off)

Pyrolysis yield and mass loss (burn-off) are key parameters for evaluating the efficiency of converting corncob into activated carbon. For each type of carbon (RMA-2M-400, RMA-2M-500, RMA-2M-600), the values were determined in triplicate (n = 3) and reported as averages. The results (Table 1) show that mass loss increases with activation temperature, while yield decreases, consistent with the findings of Lua et Yang (2004) and Ioannidou and Zabaniotou (2007). This decrease in yield is attributed first to the primary decomposition of the biomass and subsequently to the secondary decomposition of the carbonaceous residues (Ioannidou and Zabaniotou 2007). The yields obtained range from 39.37% to 58.62%. Mass losses greater than 50% were observed at 600 °C, while between 400 and 500 °C they remained below 50%.

**Table 1.** Mass loss and pyrolysis yield of corncob

| Activation temperature | Samples | **Mass loss** $\Delta m(g)$ | **Yield after pyrolysis (corn cobs)** (Rdt (%) ± SD) |
|---|---|---|---|
| 400 °C | RMA-2M-400 | 41.37 **± 0,18%** | **58.62 ± 0,18%** |
| 500 °C | RMA-2M-500 | 45.27 **± 0,22** | **54.72 ± 0,22** |
| 600 °C | RMA-2M-600 | 60.62 **± 0,20** | **39.38 ± 0,20** |

The burn-off represents the fraction of organic matter removed during chemical activation. The measured values are 41.37% (RMA-2M-400), 45.27% (RMA-2M-500), and 60.62% (RMA-2M-600). Increasing the pyrolysis temperature leads to higher mass loss as a result of enhanced thermal degradation of lignocellulosic components (hemicellulose, cellulose, lignin). At low temperatures (200–300 °C), only a limited fraction of volatile compounds is released, whereas at higher temperatures (400–600 °C) decomposition becomes more pronounced, thereby increasing mass loss (Ioannidou and Zabaniotou 2007; Demirbas 2004).
For $H_3PO_4$ activated carbons, typical burn-off values of approximately 20–50% are frequently reported and depend on the impregnation ratio, temperature, and activation time (Ioannidou and Zabaniotou 2007; Jagtoyen and Derbyshire 1998). Orthophosphoric acid acts as a dehydrating agent, promotes the introduction of phosphorus-containing groups (confirmed by FTIR), and facilitates the development of the pore structure (Jagtoyen and Derbyshire 1998).

A burn-off in the range of 30–60% is generally associated with good development of micro-/mesopores and high adsorption capacities (Molina-Sabio et Rodríguez-Reinoso 2004; Yeo 2020), while a burn-off greater than 60% may indicate over-activation and weakening of the carbon matrix (Ioannidou and Zabaniotou 2007).
In this context, RMA-2M-400 and RMA-2M-500 (41.37% and 45.27%) fall within the favorable range. RMA-2M-600 (60.62%) is at the upper threshold, suggesting increased pore opening (higher mesoporosity and possible emergence of macropores) and a potential risk of over-activation.
After pyrolysis, the measured yields are 58.62% (RMA-2M-400), 54.72% (RMA-2M-500), and 39.37% (RMA-2M-600). Yield, defined as the ratio of the mass of carbon obtained to the initial biomass mass, decreases as temperature increases, reflecting greater mass losses. At high temperatures, thermolabile organic compounds volatilize, reducing the amount of residual carbonaceous material (Lua and Yang 2004). The resulting material (activated carbon) is lightweight, highly porous, and rich in carbon (Allaire and Lange, 2013). Consequently, higher pyrolysis temperatures produce more porous activated carbons with higher fixed carbon content, but in smaller quantities (Lua et Yang 2004).
The yield of 54.72% obtained at 500 °C with $H_3PO_4$ is slightly higher than the value reported by Rodríguez Arana and Mazzoco (2010) (48.16%) for black cherry shells impregnated with phosphoric acid and activated between 500 and 550 °C. This difference may be attributed to the concentration of the activating agent and the nature of the biomass, two parameters known to influence yield (Kouadio and al. 2022). Furthermore, (Rodríguez Arana and Mazzoco 2010) reported that, under $H_3PO_4$ activation, optimal carbonization temperatures generally lie between 500 and 550 °C.

### 3.2. Specific surface area

The specific surface area of the activated carbons prepared from corncob and activated at different temperatures was determined using the methylene blue method, based on equation (5). The results obtained are summarized in Table 2 below.

**Table 2.** Specific surface area of corncob-based activated carbons as a function of activation temperature

| **Sample** | **$Q_m$ ($mg.g^{-1}$)** | **$S_L$ ($m^2.g^{-1}$)** |
|---|---|---|
| RMA-2M-400 °C | 62.11 | 93.79 |
| RMA-2M-500 °C | 1250.00 | 1887.45 |
| RMA-2M-600 °C | 344.83 | 520.68 |

These results show a clear influence of activation temperature on the maximum adsorption capacity and the specific surface area of the activated carbon.
The evolution of the specific surface area as a function of temperature reveals a characteristic trend. At 400 °C, the specific surface area remains relatively low (93.79 $m^2 \cdot g^{-1}$), indicating incomplete activation and limited pore opening. Increasing the temperature to 500 °C results in a marked increase in surface area, reaching 1887.45 $m^2 \cdot g^{-1}$. This high value indicates that activation at 500 °C promotes the development of an optimal porous structure, consistent with findings from similar studies conducted on lignocellulosic biomasses activated with $H_3PO_4$ (Liou 2010; Demiral et Aydin Şamdan 2016). In a related study, Han and al. (2020) reported a methylene blue adsorption capacity of 977 $mg.g^{-1}$ for activated carbons produced from eucalyptus residues treated with phosphoric acid, confirming the effectiveness of $H_3PO_4$ activation in generating highly porous and efficient materials.

In contrast, when the temperature reaches 600 °C, the specific surface area decreases significantly to 520.68 $m^2.g^{-1}$. This reduction can be attributed to excessive decomposition of the carbon matrix and partial fusion of the pore walls, leading to the collapse of the microporous structure (Ioannidou et Zabaniotou 2007). This behavior is well documented in the literature: beyond a critical temperature, the specific surface area tends to decrease due to pore contraction and excessive volatilization of organic components (Marsh, Harry; Rodríguez Reinoso, 2006).
The results obtained confirm that activation temperature plays a decisive role in the development of porosity in activated carbons. Activation at 500 °C appears to be the most favorable condition for corncob, providing the material with a high specific surface area and thus a strong adsorption potential.

### 3.3. Ash content, moisture content, and $pH_{PZC}$

The sample RMA-2M-500, which exhibited the highest specific surface area and the best pollutant removal efficiency, was selected for the determination of ash content, moisture content, and the point of zero charge ($pH_{PZC}$). The results obtained are presented in Table 3. The determination of $pH_{PZC}$ is illustrated in Figure 1.
**Table 3.** Ash content, moisture content, and $pH_{PZC}$ values for the RMA-2M-500 activated carbon sample.

| **Settings** | **Activated carbon** | **Normative references** |
|---|---|---|
| **Humidity (%)** | 4.93 | 3 – 8 (max 10%) |
| **Ash (%)** | 9.8 | 2 – 10 % (max 15%) |
| **$pH_{PZC}$** | 3.4 | - |

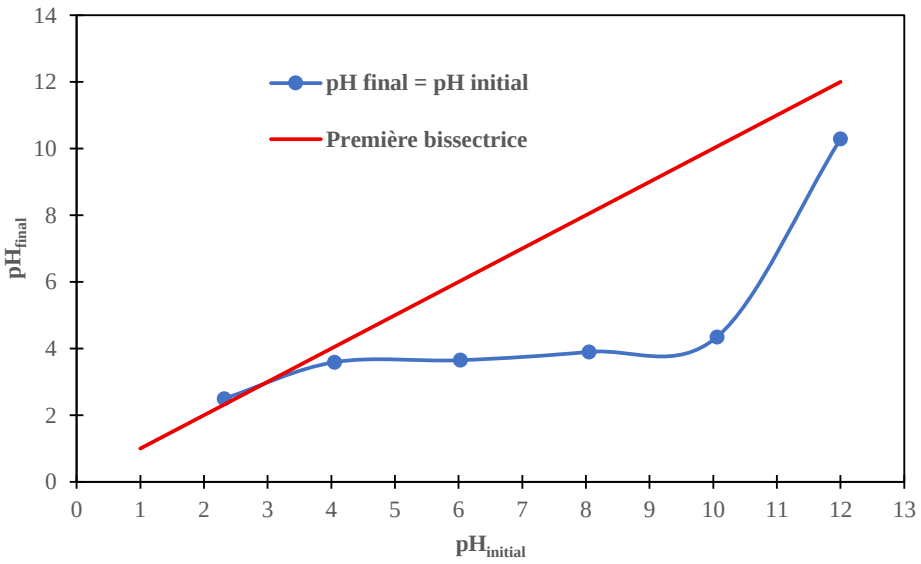


**Figure 1:** Determination of pH at zero loading point ($pH_{PZC}$), contact time: 72 h, 350 rpm.

The measured $pH_{PZC}$ of 3.4 indicates an acidic surface character: the net surface charge of the RMA-2M-500 activated carbon is zero at pH = 3.4, where positive and negative surface charges compensate each other (Bansal and Goyal 2005). This behavior is typical of $H_3PO_4$-activated lignocellulosic biomass–derived activated carbons, in which the presence of acidic groups (carboxyl, phenolic, phosphate) lowers the $pH_{PZC}$. Several studies have confirmed the acidic nature of the surfaces of $H_3PO_4$-activated lignocellulosic carbons, with $pH_{PZC}$ values generally ranging between 2 and 4 (Bansal and Goyal 2005; Moreno-Castilla 2004).
Alhawtali and al. (2024) reported a $pH_{PZC}$ of 2.39 for carbon microspheres derived from date-palm leaves and activated with $H_3PO_4$, while Mandal and al. (2024) reported $pH_{PZC}$ values ranging from 3.6 to 3.8 for activated carbons produced from peanut shells and areca fibers treated with $H_3PO_4$.
Surface speciation therefore depends on the solution pH: for pH > 3.4, the surface becomes predominantly negative and favors the adsorption of cations; for pH < 3.4, it becomes positively charged and favors the adsorption of anions (Daifullah and al. 2004; Mohan and Pittman 2007). FTIR analysis confirms the presence of acidic functional groups on the materials studied.
Ash content and moisture content are major parameters in the characterization of activated carbons. According to ASTM Standard D2866 (D28 Committee, s. d.), ash content corresponds to the mineral fraction remaining after complete combustion of the carbon at high temperature. The measured value (9.8%) falls within the recommended range for good-quality activated carbon (2–10%, max. 15%). A high ash content can reduce the specific surface area by occupying pores or increasing the inert fraction (Patnukao et Pavasant 2008).
Moisture content (or residual moisture), expressed as a percentage of mass, reflects the amount of water retained within the material. The value obtained (4.93%) is low, indicating effective drying; it is consistent with common recommendations (3–8%, max. 10%) (Foo et Hameed 2010). This parameter directly affects stability, storage, and adsorption performance. Excessively high moisture content can reduce adsorption capacity by occupying or temporarily blocking micropores, thereby preventing target molecules from accessing them (Bansal and Goyal 2005; Foo and Hameed 2010).

### 3.4. FTIR analysis

Fourier Transform Infrared (FTIR) spectroscopy revealed the presence of several functional groups characteristic of the activated carbon surface. The spectrum corresponding to the RMA-2M-500 activated carbon is shown in Figure 2, where the main absorption bands associated with these functional groups can be observed.

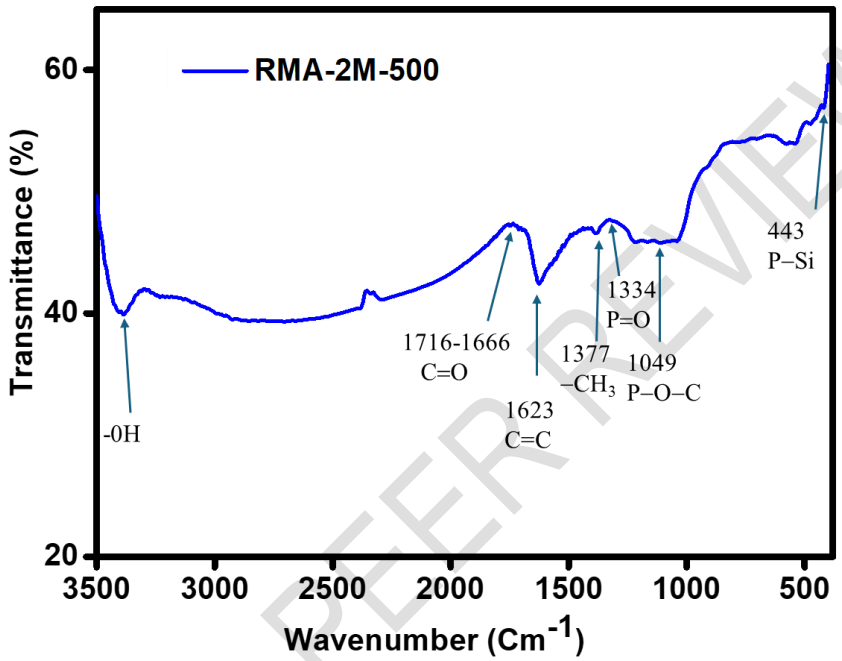


**Figure 2.** Fourier Transform Infrared (FTIR) spectrum of corncob-based activated carbon produced at 500 °C using 2 M $H_3PO_4$

The FTIR spectrum shows bands around ~3400 $cm^{-1}$ corresponding to O–H stretching vibrations, likely arising from adsorbed water or phenolic groups (Yakout et Sharaf El-Deen 2016; Coates 2000; Kriz Pavia, 2001). This feature reflects weakly to moderately hydrogen-bonded O–H stretches, consistent with phenolic or alcoholic groups, as well as weakly bridged carboxylic O–H groups when the broad continuum typical of strongly hydrogen-bonded acids is absent (Socrates 2001)

Bands located between 1716 and 1666 $cm^{-1}$ are characteristic of carbonyl (C=O) groups, particularly those associated with aromatic acidic functionalities (Coates 2000; Silverstein, Webster & Kiemle, 2025). Similar O–H and C=O signatures have been reported for biomass-derived chars by Abdulqader and al. (2024) and Jawad and al. (2016), supporting these assignments for the corncob-derived activated carbons.

Phosphorus-containing groups resulting from $H_3PO_4$ activation are evidenced by the band near 1049 $cm^{-1}$, attributed to P–O–C, along with components around 1334 $cm^{-1}$ corresponding to P=O vibrations (Abdulqader and al. 2024; Alhawtali and al. 2024). Low-frequency modes between 460 and 440 $cm^{-1}$ suggest phosphate-related contributions and the possible formation of Si–P bonds (Figure 2.f) in the presence of native silica from the corncob, a phenomenon expected during phosphate–silica condensation processes (Abdulqader et al. 2024; Gottipati 2012; Sangoremi 2025).

7) Please mention A,B,C,D,E,F,and G on the picture/figure2 because the author did not mention on the picture/figure2

The aromatic C=C stretching observed at 1623 $cm^{-1}$ confirms the development of an aromatic/graphitic carbon framework during thermal treatment. The band at 1377 $cm^{-1}$ indicates the presence of $CH_3$ groups (Marsh, Harry; Rodríguez Reinoso, Francisco, 2006). Rich in functional groups, these activated carbons exhibit strong affinity toward cationic dyes (including methylene blue) and enhance the adsorption of both metallic and organic pollutants, owing to the combination of their acidic, oxygenated, and phosphorus-containing surface functionalities.

### 3.6. SEM–EDS analysis

The EDS results for the RMA-2M-500 activated carbon (Table 4, Figure 3) show a well-defined organization of the surface composition. Phosphorus appears at approximately 4.7 wt % (2.1 at.%), confirming the incorporation of phosphate groups into the carbon matrix. Carbon reaches nearly 65 wt % (73 at.%), indicating an enrichment in aromatic structures, while oxygen accounts for about 28 wt % (24 at.%). Mineral elements such as calcium and silica persist only as trace components.

**Table 4.** Elemental composition of corncob-based activated carbon activated with phosphoric acid ($H_3PO_4$).

| Element | Weight % | Weight % Error | Atom % | Atom % Error |
|---|---|---|---|---|
| **C** | 64.9 | ± 0.5 | 73.2 | ± 1.2 |
| **O** | 28.3 | ± 0.7 | 24.0 | ± 1.2 |
| **Si** | 0.5 | ± 0.1 | 0.3 | ± 0.1 |
| **P** | 4.7 | ± 0.2 | 2.1 | ± 0.1 |
| **Ca** | 1.6 | ± 0.2 | 0.5 | ± 0.1 |
| **Total** | 100.0 | | 100.0 | |

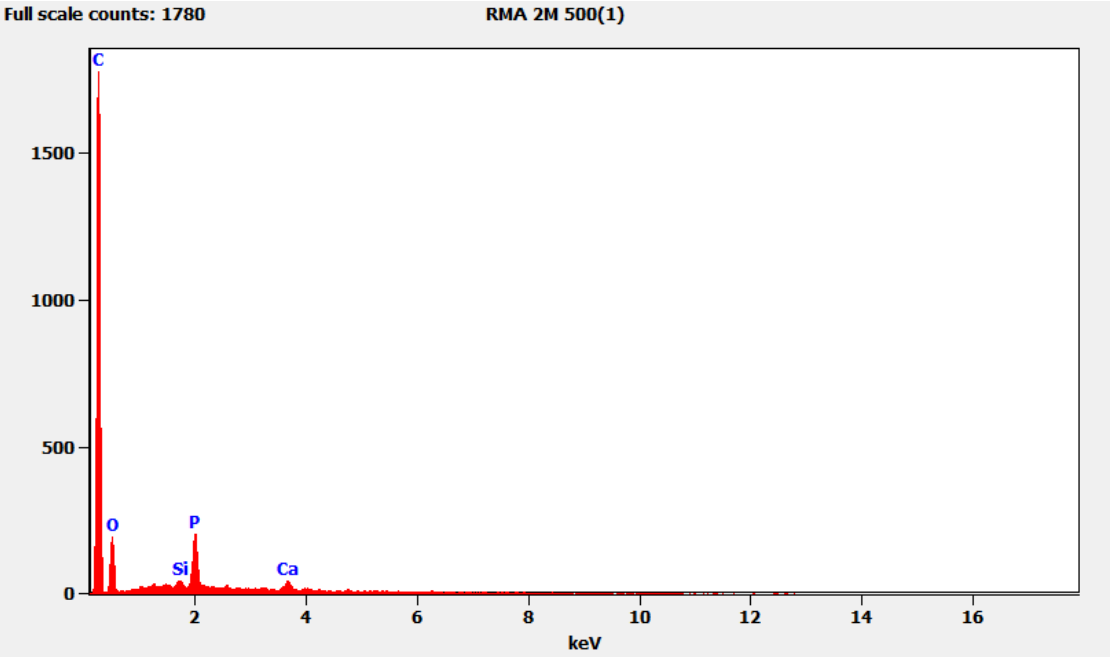


**Figure 3.** EDS spectrum of the RMA-2M-500 activated carbon produced with $H_3PO_4$, confirming phosphorus incorporation.

Following impregnation and activation with $H_3PO_4$, the observed modifications confirm the key role of the chemical activating agent. The high carbon content and the presence of oxygen indicate the formation of more stable aromatic carbon structures (Liou 2010). The appearance of phosphorus on the surface reveals the presence of phosphate groups, which enhance the adsorption of oxyanions and metal cations through mechanisms such as complexation, precipitation, or electrostatic interactions (Wang et al. 2017; Pan et al. 2022).
The SEM micrographs of the activated carbon (Figure 4) highlight a pronounced morphological transformation characterized by the emergence of numerous cavities, cracks, and interconnected pores, giving the material a heterogeneous and porous structure.

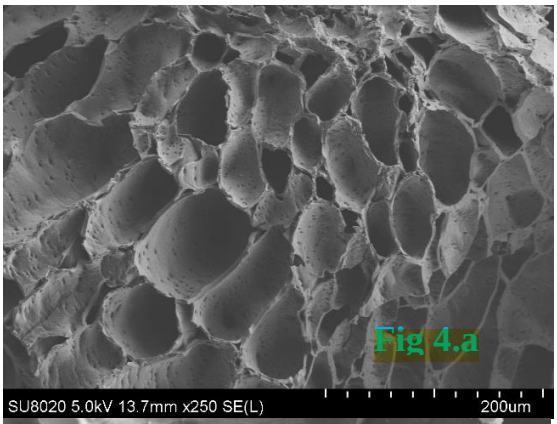


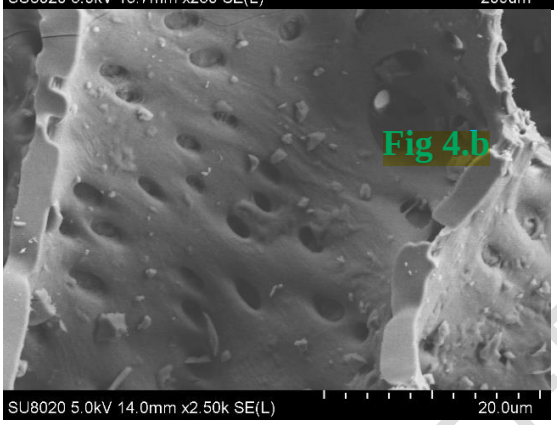




**Figure 4 (a, b):** SEM micrograph of activated carbon showing hierarchical porosity (micropores, mesopores, and macropores)

The SEM micrographs confirm the structural transformations occurring on the surface of the activated carbons: the surface is rough, cracked, and porous. This morphology is characteristic of the action of phosphoric acid, which induces dehydration and the formation of internal channels within the carbon matrix (Yakout et Sharaf El-Deen 2016). The persistent presence of silica and calcium, even at trace levels, may also influence surface reactivity, as several authors have reported that these elements can compete with cations such as $Pb^{2+}$ or interact with oxyanions such as $AsO_4^{3-}$ (Mitra et al. 2019).

With regard to porosity, the SEM micrographs of the activated carbon reveal the coexistence of micropores (< 2 nm), mesopores (2–50 nm), and macropores (> 50 nm). Micropores contribute to increasing the specific surface area and provide a high adsorption capacity for small molecules such as arsenic. Mesopores facilitate the diffusion and accessibility of larger ions, particularly lead. Finally, macropores act as transport channels, allowing improved fluid circulation through the adsorbent bed (Liou 2010; Marsh, Harry; Rodríguez Reinoso, Francisco, 2006). This hierarchical porosity endows the activated material with dual efficiency: rapid adsorption kinetics due to the meso/macropores and high adsorption capacity resulting from the micropores.

These results therefore confirm that impregnation and activation with $H_3PO_4$ profoundly transform the chemical and morphological structure of the material, making the activated carbon more porous, richer in phosphate-containing sites, and better suited for the adsorption of metal pollutants and metal–oxyanion species.

With regard to porosity, the SEM micrographs of the activated carbon show the coexistence of micropores (< 2 nm), mesopores (2–50 nm), and macropores (> 50 nm). Micropores

8) Repeated

increase the specific surface area and enhance the adsorption capacity for small species, including methylene blue and certain metalloids such as arsenic. Mesopores facilitate intraparticle diffusion and improve accessibility for larger molecules such as methylene blue, as well as for heavy ions such as lead. Macropores act as transport channels, improving fluid circulation within the adsorbent bed bed (Liou 2010; Marsh, Harry; Rodríguez Reinoso, Francisco, 2006). This hierarchical porosity combines rapid adsorption kinetics—thanks to the meso/macropores—with high adsorption capacity provided by the micropores, which is particularly favorable for methylene blue removal.

These results confirm that impregnation and activation with $H_3PO_4$ deeply transform the surface chemistry and morphology of the material, making the carbon more porous, richer in phosphate-containing sites, and better suited for the adsorption of cationic organic pollutants such as methylene blue, as well as metallic and oxyanion pollutants. The enrichment in acidic/oxygenated functionalities and phosphorus-containing groups, combined with the aromatic carbon framework, promotes electrostatic and π–π interactions with methylene blue, thereby enhancing both the kinetics and the adsorption capacity (Alhawtali and al. 2024; Mandal and al. 2024).

## 3.6. Adsorption performance assessment

### 3.6.1. Thermodynamic analysis

The Van't Hoff equation (10) and the Gibbs–Helmholtz equation (11) were used to determine the thermodynamic parameters.

$$\ln K_d = -\frac{\Delta H^\circ}{R} \times \frac{1}{T} + \frac{\Delta S^\circ}{R} \quad (10)$$

$$\Delta G^\circ = \Delta H^\circ - T\Delta S^\circ \quad (11)$$

Where $K_d = \frac{Q_e}{C_e}$ is the distribution coefficient, R (8.314 J.mol$^{-1}$ K$^{-1}$) is the ideal gas constant, and T is the absolute temperature of the solution in Kelvin (K); $Q_e$ (mg.g$^{-1}$) is the quantity adsorbed at equilibrium and Ce (mg.L$^{-1}$) is the concentration at equilibrium. Plotting the $\ln K_d$ curve as a function of $\frac{1}{T}$ gives the values of ΔH° and ΔS°; the slope being $-\frac{\Delta H^\circ}{R}$ and the y-intercept $\frac{\Delta S^\circ}{R}$. ΔG° is determined using the values ΔH° and ΔS°. The thermodynamic parameters are shown in Table 4a.

**Table 4a.** Thermodynamic parameters

| T (K) | ΔG° (J. mol$^{-1}$) | ΔH° (J. mol$^{-1}$) | ΔS° (J. mol$^{-1}$. K$^{-1}$) |
|---|---|---|---|
| 305,15 | - 4645,174 | 29 200,431 | 110,643 |
| 320,15 | - 6221,833 | | |
| 334,15 | - 7770,831 | | |

The analysis of the thermodynamic parameters provides deeper insight into the nature and feasibility of the adsorption process. The values obtained were ΔH° = 29.20 kJ.mol$^{-1}$ and ΔS° = 110.64 J·mol$^{-1}$.K$^{-1}$. The positive standard enthalpy (ΔH° > 0) indicates that the adsorption is endothermic; thus, increasing temperature enhances the adsorption of methylene blue onto the prepared activated carbons. The relatively low enthalpy (29.20 kJ.mol$^{-1}$, i.e., < 40 kJ.mol$^{-1}$) is consistent with a physisorption process (Baari et al. 2025).

Moreover, the positive entropy value (ΔS° > 0) suggests an increase in disorder at the solid–liquid interface, which can be attributed to the disruption of the solvation shell of water in favor of solute–adsorbent site interactions (Boumchita et al. 2016; Foo et Hameed 2010; Haghseresht et Lu 1998). This also reflects a strong affinity between the cationic dye and the carbon surface (Basu et al. 2018).
From ΔG° = ΔH° − TΔS°, all ΔG° values were negative over the temperature range investigated, indicating that the adsorption process is spontaneous and thermodynamically favorable (Basu et al. 2018). Altogether, these results confirm the effectiveness of phosphoric-acid-activated carbons under typical water-treatment temperatures.

### 3.6.2. Langmuir model

Figure 5 shows the Langmuir isotherms for the adsorption of methylene blue (MB) onto corncob-based activated carbons produced at 400, 500, and 600 °C (impregnation with 2.0 M $H_3PO_4$), using 0.05 g of adsorbent in 80 mL of MB solution at pH 6.68.

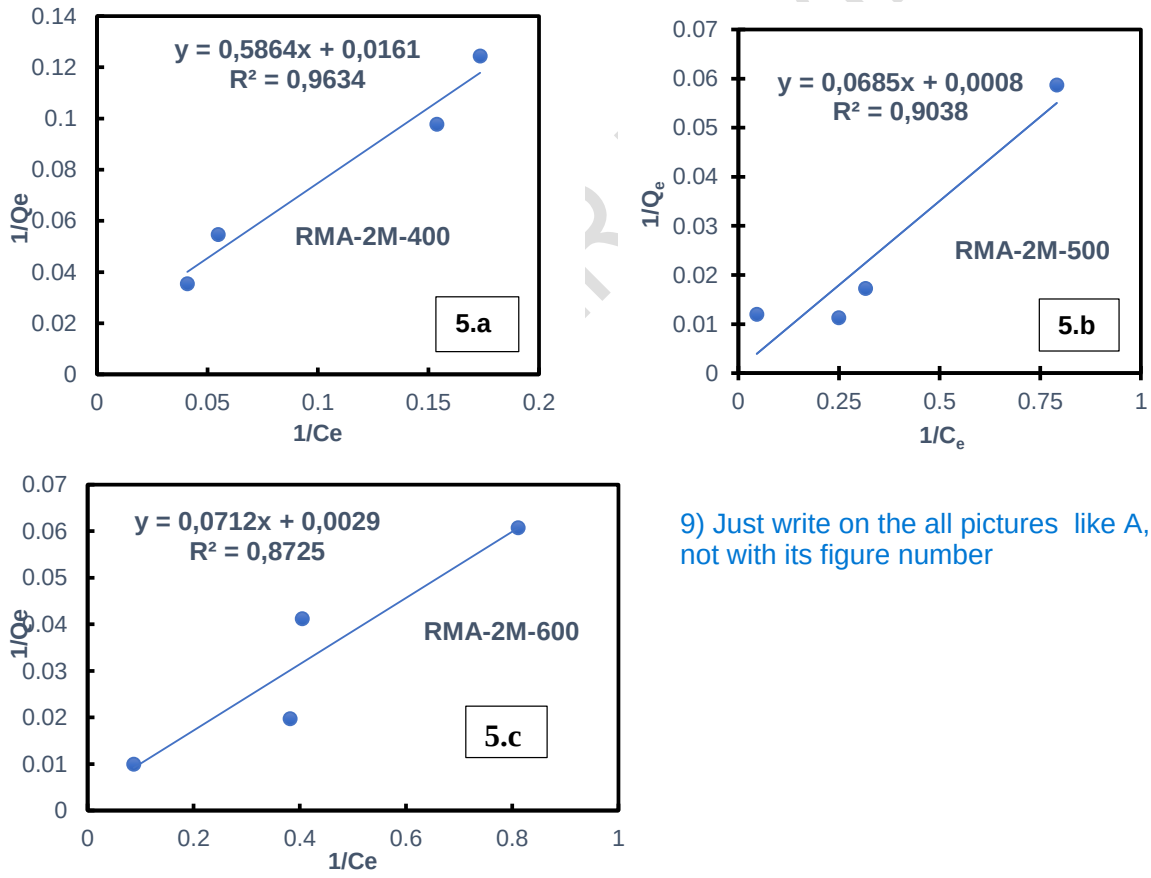


9) Just write on the all pictures like A,B, and C not with its figure number

**Figure 5 (a,b,c):** Langmuir adsorption of corn cobs activated carbon toward BM as a function of activation temperature

The two equilibrium parameters, $K_L$ and $Q_{max}$, obtained from the Langmuir model are presented in Table 5.
The dimensionless separation factor $R_L$, which indicates whether the adsorption process is favorable or not, is defined by equation (12):

$$R_L = \frac{1}{1 + K_L C_0} \qquad (12)$$

where $C_0$ (mg.g$^{-1}$) denotes the initial concentration of the pollutant and $K_L$ (L.mg$^{-1}$) denotes the Langmuir constant.

**Table 5:** Langmuir constants determined from the lines $\frac{1}{Q_e} = f\left(\frac{1}{C_e}\right)$.

| Samples | Langmuir model | | | | |
|---|---|---|---|---|---|
| | $Q_m$ (mg.g$^{-1}$) | $K_L$ (L.mg$^{-1}$) | $R_L$ | $R^2$ | $S_L$ (m².g$^{-1}$) |
| **RMA-2M-400** | 62.11 | 0.0274 | 0.59 | 0,963 | 93.79 |
| **RMA-2M-500** | 1250.00 | 0.0116 | 0.66 | 0,904 | 1887.45 |
| **RMA-2M-600** | 344.83 | 0.0407 | 0.68 | 0,872 | 520.68 |

10) Please mention the SL under the table

The application of the Langmuir isotherm to the experimental data made it possible to evaluate the maximum adsorption capacity of the activated carbons produced from corncob, as well as their affinity toward the adsorbate. The results show a strong influence of activation temperature on the model parameters. The maximum adsorption capacity $Q_m$ varies considerably among the samples, reaching 1250 mg·g$^{-1}$ for RMA-2M-500, compared with only 62.11 mg.g$^{-1}$ at 400 °C and 344.83 mg.g$^{-1}$ at 600 °C. This exceptional value obtained at 500 °C reflects the optimal development of microporosity and the high specific surface area (1887.45 m².g$^{-1}$), conditions that are particularly favorable for adsorption (Liou 2010; Freundlich 1907). These observations confirm that activation temperature is a key parameter governing the performance of activated carbons.

The analysis of the Langmuir constant ($K_L$) shows values ranging from 0.0116 to 0.0407 L.mg$^{-1}$, indicating a moderate affinity between the activated carbon and the adsorbate. The RMA-2M-600 sample exhibits the highest value ($K_L$=0.0407), suggesting stronger interactions, although its maximum adsorption capacity remains lower than that of RMA-2M-500. This contrast illustrates that the constant $K_L$ reflects not only the number of available adsorption sites but also the nature of the interactions between the surface and the solute (Foo et Hameed 2010).

The separation factor ($R_L$), used to assess the favorability of the adsorption process, exhibits values between 0.59 and 0.68. According to the criterion established by (Foo et Hameed 2010; Basu et al. 2018), values between 0 and 1 indicate favorable adsorption, confirming the effectiveness of all three samples for the system studied.

The Langmuir model fits the data well for RMA-2M-400 ($R^2$=0.963) and RMA-2M-500 ($R^2$=0.904). The slightly lower yet still high $R^2$ at 500 °C may indicate increased heterogeneity of the material at this temperature. For the sample activated at 600 °C, the model provides the weakest fit, with $R^2$=0.872.

The consistency between the specific surface area values ($S_L$) and the maximum adsorption capacity ($Q_m$) is also noteworthy. The RMA-2M-500 sample, which exhibits the highest specific surface area (1887.45 m²·g$^{-1}$), is also the one that displays the highest adsorption capacity.

This correlation reinforces the idea that the performance of activated carbons is closely linked to the development of their porosity and the availability of active sites.
Overall, the Langmuir isotherm confirms that RMA-2M-500 is the most efficient activated carbon, combining high adsorption capacity, favorable adsorption behavior, and a good fit to the model. These results are consistent with the literature, which reports that phosphoric-acid-activated carbons generally achieve their best performance within a temperature range around 500 °C (Liou 2010; Freundlich 1907).

### 3.6.3. Freundlich model

The plots in Figure 6 illustrate the adsorption behavior described by the Freundlich model for methylene blue (MB) on corncob-based activated carbons activated at 400 °C, 500 °C, and 600 °C, using an activating agent concentration of 2 M, 0.05 g of adsorbent, and 80 mL of MB solution at pH 6.68.

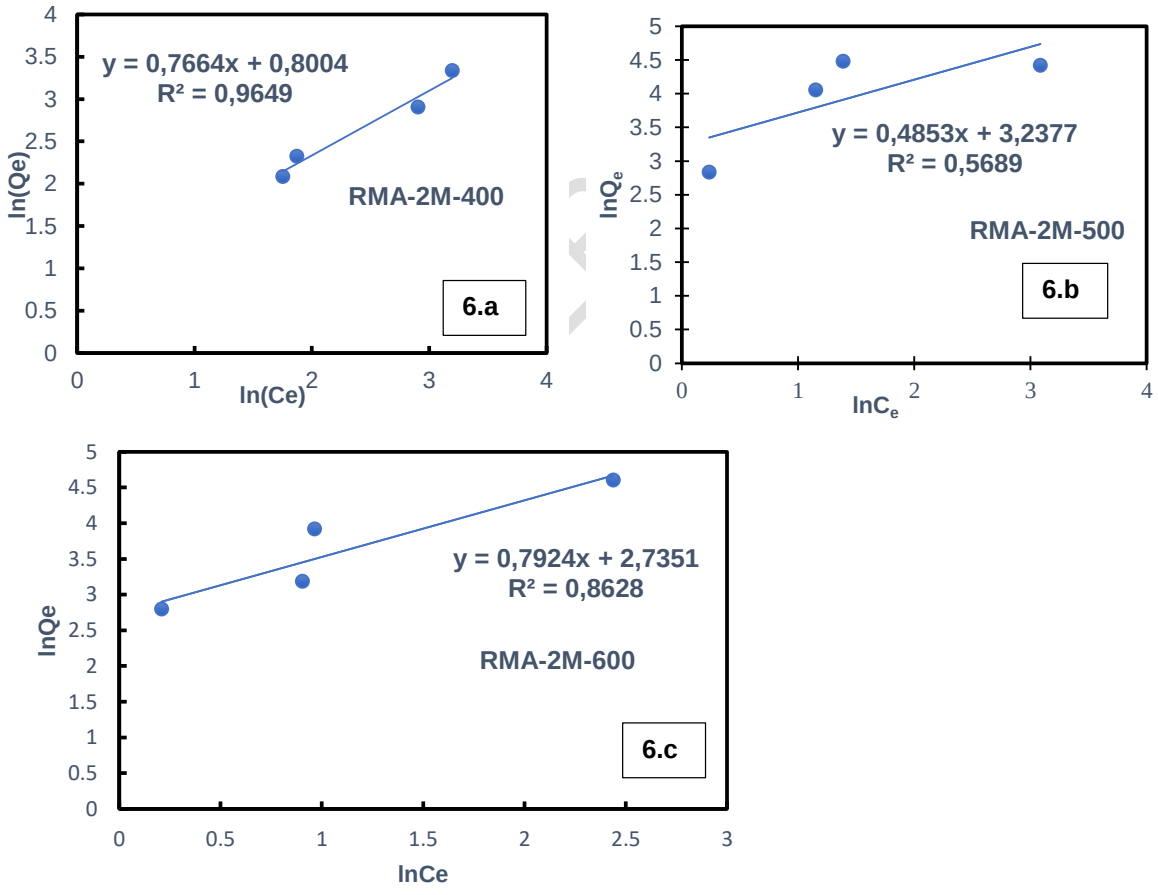


**Figure 6 (a, b, c):** Adsorption according to Freundlich's model of corn cob hulls (CA-Rafle) with respect to BM as a function of activation temperature.

The constants $K_F$ and $\frac{1}{n_F}$ are determined using the linear form of the Freundlich isotherm (Equation 9) and recorded in Table 6.

**Table 6:** Freundlich constants determined from the straight lines $\ln Q_e = f(\ln C_e)$.

| Samples | Freundlich model | | |
|---|---|---|---|
| | $\frac{1}{n_F}$ | $K_F$ (L.g$^{-1}$) | $R^2$ |
| **RMA-2M-400** | 0.766 | 2.226 | 0.964 |
| **RMA-2M-500** | 0.485 | 25.475 | 0.569 |
| **RMA-2M-600** | 0.792 | 15.411 | 0.863 |

The results show that the constant $K_F$, which reflects the adsorption capacity, varies strongly with activation temperature. The RMA-2M-500 sample exhibits the highest value ($K_F$=25.475 L.g$^{-1}$), indicating a strong adsorption capacity, whereas the samples activated at 400 °C ($K_F$=2.226 L.g$^{-1}$) and 600 °C ($K_F$=15.411 L.g$^{-1}$) display significantly lower performance. This trend is consistent with the Langmuir model results, confirming that an activation temperature of 500 °C provides a pore structure and surface chemistry more favorable for adsorption (Liou 2010; Freundlich 1907).

The parameter $\frac{1}{n_F}$ , which indicates the intensity and favorability of adsorption, ranges from 0.485 to 0.792. All samples exhibit values of $\frac{1}{n_F}$ <1, which indicates favorable adsorption on the activated carbons and strong adsorbent–adsorbate interactions (Boumchita et al. 2016).

Regarding the quality of fit, the correlation coefficient ($R^2$) ranges from 0.569 to 0.964. The best fit is obtained for RMA-2M-400 ($R^2$=0.964), followed by RMA-2M-600 ($R^2$=0.863), whereas the RMA-2M-500 sample exhibits a very poor fit ($R^2$=0.569). This indicates that, despite its excellent performance in terms of adsorption capacity ($K_F$) and favorability ($\frac{1}{n_F}$), the RMA-2M-500 sample is not well described by the Freundlich model. This result suggests that, for this sample, the adsorption mechanism is more homogeneous and better represented by the Langmuir model, which assumes monolayer adsorption on a uniform surface (Harry Marsh, Francisco Rodríguez Reinoso, 2006).

Overall, the application of the Freundlich model shows that RMA-2M-500 maintains the highest adsorption performance, but its behavior is more accurately described by the Langmuir model. The samples activated at 400 and 600 °C exhibit more heterogeneous adsorption, which explains their better fit to the Freundlich model. This complementarity between the two models highlights the importance of comparative analysis for a more comprehensive description of adsorption phenomena (Haghseresht et Lu 1998; M. Vargas-Rodríguez et al. 2021).

Following the analysis of adsorption isotherms which provided insight into maximum capacity and process favorability it is necessary to examine the dynamic retention of the adsorbate to better understand the mechanisms involved. The study of adsorption kinetics provides essential information on the rate of the process and the steps controlling mass transfer, enabling evaluation of the activated carbon's efficiency over time.

### 3.6.4. Pollutant removal efficiency

To determine the removal efficiency of methylene blue (MB) by the activated carbons, 80 mL of a cationic dye solution with an initial concentration of 42 mg.L$^{-1}$ were brought into contact with each sample and agitated for 90 minutes, corresponding to the equilibrium time. The removal efficiency R (%) was calculated using equation (13), and the results for the three activated carbon samples are shown in Figure 7.

$$R(\%) = \frac{C_i - C_e}{C_i} \times 100 \qquad (13)$$

Where R(%) is the removal efficiency; $C_i$ is the initial concentration in mg.L$^{-1}$; $C_e$ is the residual concentration in mg.L$^{-1}$ at a given time t.

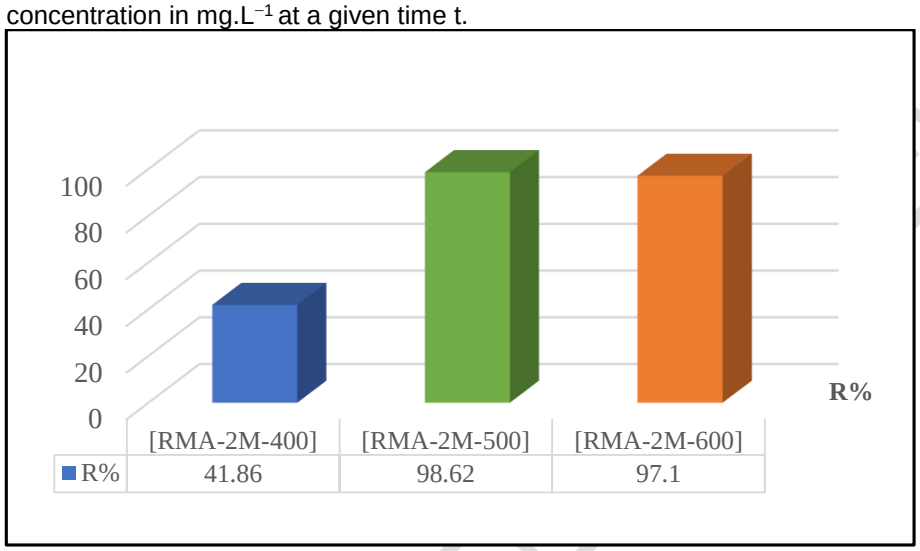


**Figure 7**: Methylene blue removal efficiency as a function of pyrolysis temperature (400–600 °C) of corn stover CA samples activated with $H_3PO_4$ at 90 minutes.

The removal of methylene blue was monitored using UV–Visible spectrophotometry. Figure 8 shows the superimposed spectra of the dye alone and those recorded after 60 minutes of contact with the activated carbons RMA-2M-400, RMA-2M-500, and RMA-2M-600. This comparison highlights the decrease in methylene blue absorbance after treatment, illustrating the adsorption efficiency of the materials.

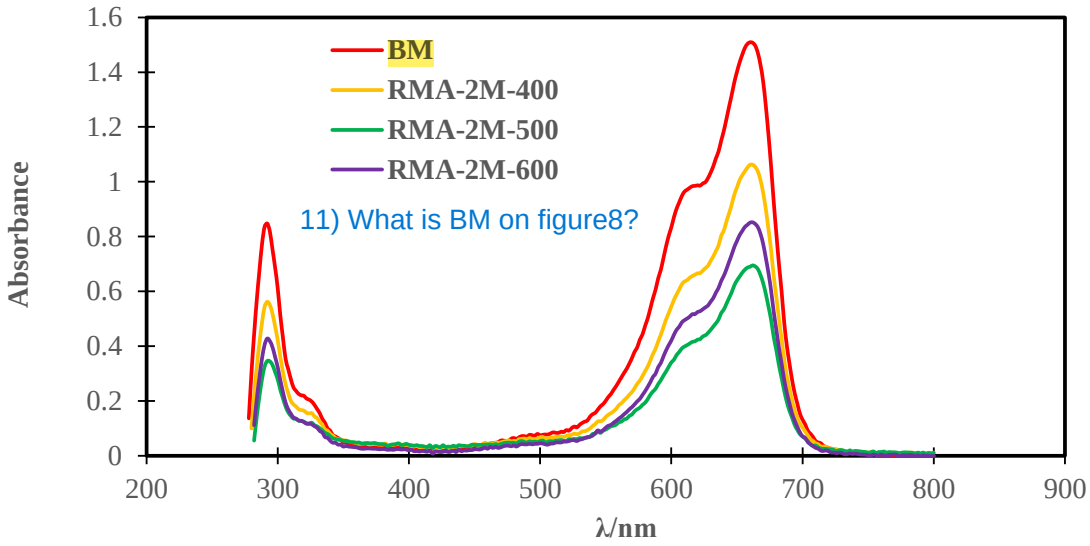


**Figure 8:** UV-Visible adsorption spectra of methylene blue alone (red), MB + RMA-2M-400 (yellow), MB + RMA-2M-500 (green), and MB + RMA-2M-600 (purple) after 60 minutes of treatment.

At contact times of 0, 60, 80, and 90 minutes, Figure 9 shows the UV–Visible absorption spectra of methylene blue in the presence of RMA-2M-500. The progressive decrease in absorbance over time reflects the increasing removal of the dye by this activated carbon.

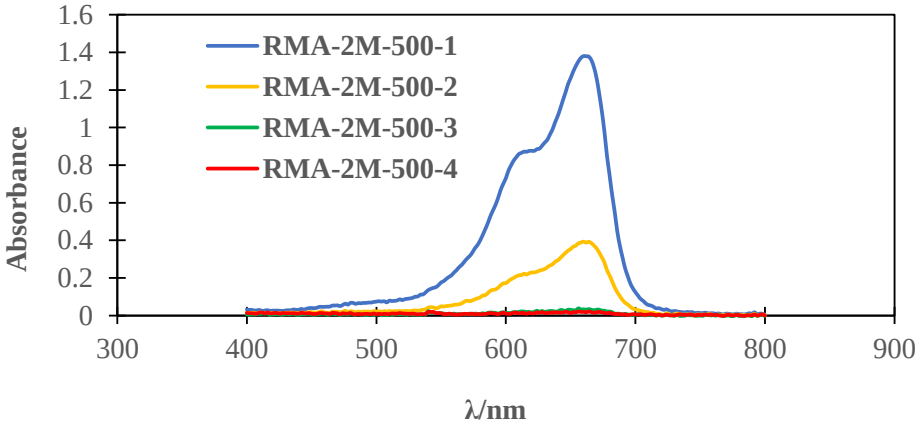


**Figure 9:** UV-Visible absorption spectra illustrating the removal of methylene blue by CA RMA-2M-500 after 90 minutes of treatment. RMA-2M-500-1 (t = 0 min, blue), RMA-2M-500-2 (t = 60 min, yellow), RMA-2M-500-3 (t = 80 min, green), and RMA-2M-500-4 (t = 90 min, red).

The effectiveness of the activated carbons was evaluated through the removal efficiency of methylene blue (Figure 7). The results show marked differences depending on the activation temperature. The RMA-2M-500 sample exhibits the highest removal efficiency at 98.62%, followed by RMA-2M-600 at 97.1%, whereas RMA-2M-400 displays a much lower efficiency of only 41.86%. These differences can be attributed to the structural and textural development of the activated carbon. At 500 °C, chemical activation with $H_3PO_4$ leads to optimal opening of micropores, which promotes the diffusion of methylene blue molecules and their attachment

to active sites—thus explaining the near-complete removal efficiency observed (Liou 2010; Freundlich 1907).
The sample activated at 600 °C also maintains a high removal efficiency, although slightly lower than that of the 500 °C sample. This may be related to partial destabilization of the carbon structure at excessively high temperatures (Demiral et Aydin Şamdan 2016).
The UV–Visible spectra (Figure 8) support these observations. After 60 minutes of treatment, a marked decrease in the characteristic methylene blue peak is observed for the RMA-2M-500 and RMA-2M-600 samples, whereas the RMA-2M-400 sample still exhibits significant absorbance, indicating lower dye removal.
Furthermore, the evolution of the spectra over time for the RMA-2M-500 sample (Figure 9) illustrates the rapid kinetics of the process: the progressive decrease in peak intensity between 60 and 90 minutes shows that adsorption is nearly complete within the first hour. This result is consistent with the kinetic studies, which already indicated fast adsorption followed by stabilization at equilibrium.
Overall, these results confirm that the optimal activation temperature is 500 °C, under which the pore structure and functional groups provide the activated carbon with maximum adsorption capacity and removal efficiency. These findings corroborate previous reports on the adsorption of organic dyes by biomass-derived activated carbons, highlighting the importance of textural and functional properties in achieving removal efficiencies above 95% (Foo et Hameed 2010).

## 4. CONCLUSION

This study demonstrates that corncob can be converted into activated carbons through chemical activation with orthophosphoric acid ($H_3PO_4$), yielding a hierarchically structured texture and surface chemistry well suited for adsorption in aqueous media. FTIR analysis revealed the presence of acidic oxygenated functions (–OH, C=O) and phosphorus-containing groups (P–O–C, P=O, P–O), while SEM observations showed the coexistence of micropores, mesopores, and macropores; EDS confirmed the incorporation of phosphorus and the presence of silica, consistent with Si–P bonding.
This combination of surface functional groups and hierarchical porosity promotes electrostatic and π–π interactions with methylene blue and reconciles access kinetics (meso-/macropores) with adsorption capacity (micropores). Modeling showed that the adsorption isotherms are better described by the Langmuir model than by the Freundlich model, with separation factors $0 < R_L < 1$ indicating favorable adsorption and coherent $Q_{max}$ and $K_L$ parameters.
The thermodynamic examination of the sample activated at 500 °C revealed $\Delta H° = +29.20$ kJ.mol$^{-1}$ and $\Delta S° > 0$, leading to $\Delta G° < 0$ over the investigated temperature range. This indicates that adsorption is endothermic, spontaneous, and thermodynamically favorable, with predominant physisorption strengthened by surface chemistry interactions. In terms of performance, the activated carbon produced at 500 °C ($H_3PO_4$ 2 M) exhibited the highest efficiency, with a specific surface area of 1887.45 m².g$^{-1}$ and a methylene blue removal rate of 98.62%. These results confirm the relevance and suitability of this valorization pathway for water treatment applications, particularly in resource-limited contexts.

**REFERENCES**


1. Abdulqader, M. A., Suliman, M. A., Ahmed, T. A., Wu, R., Bobaker, A. M., Tiyasha, T., Yassin, M. A., & Al-Areeq, N. (2024). Conversion of Chicken Rice Waste into Char via Hydrothermal, Pyrolysis, and Microwave Carbonization Processes: A Comparative Study. AUIQ Complementary Biological System, 1(1), 1-9. https://doi.org/10.70176/3007-973X.1003
2. Abid, L. H., Mussa, Z. H., Deyab, I. F., Al-Ameer, L. R., Al-Saedi, H. F. S., Al-Qaim, F. F., Kamyab, H., Rajendran, S., Imran, A. F., & Yaseen, Z. M. (2025). Walnut Shell as a bio-activated carbon for elimination of malachite green from its aqueous solution: Adsorption isotherms, kinetics and thermodynamic studies. *Results in Chemistry*, *14*(1), 102124. https://doi.org/10.1016/j.rechem.2025.102124
3. Marsh, H., & Rodríguez Reinoso, F. (2006). Activated Carbon. Elsevier Science. https://www.elsevier.com/books/activated-carbon/marsh/978-0-08-044463-5
4. Ahmed, M. J., & Dhedan, S. K. (2012). Equilibrium isotherms and kinetics modeling of methylene blue adsorption on agricultural wastes-based activated carbons. Fluid Phase Equilibria, 317, 9–14. https://doi.org/10.1016/j.fluid.2011.12.026
5. Al-Asadi, S. T., Mussa, Z. H., Al-Qaim, F. F., Kamyab, H., Al-Saedi, H. F. S., Deyab, I. F., & Kadhim, N. J. (2025). A comprehensive review of methylene blue dye adsorption on activated carbon from edible fruit seeds: A case study on kinetics and adsorption models. Carbon Trends, 20, 100507. https://doi.org/10.1016/j.cartre.2025.100507
6. Alhawtali, S., El-Harbawi, M., El Blidi, L., Alrashed, M. M., Alzobidi, A., & Yin, C.-Y. (2024). Date Palm Leaflet-Derived Carbon Microspheres Activated Using Phosphoric Acid for Efficient Lead (II) Adsorption. C, 10(1), 26. https://doi.org/10.3390/c10010026
7. ALOthman, Z. A. (2012). A Review: Fundamental Aspects of Silicate Mesoporous Materials. Materials, 5(12), 2874–2902. https://doi.org/10.3390/ma512874
8. « Article Detail ». s. d. *International Journal of Advanced Research*. Consulté le 29 novembre 2025. https://www.journalijar.com/article/.
9. Baari, M. J., Rudi, L., & Harimu, L. (2025). Adsorption isotherms, thermodynamics, and kinetics of activated carbon as adsorbent to water

pollutants: a review. Chimica Techno Acta. https://doi.org/10.15826/chimtech.2025.12.2.14

10. Bamba, D., Dongui, B., Trokourey, A., Kouassi, K., & Soro, A. (2009). Etudes comparées des méthodes de préparation du charbon actif, suivies d'un test de dépollution d'une eau contaminée au diuron. Revue des Sciences et Technologies de l'Environnement. https://www.semanticscholar.org/paper/Etudes-compar%C3%A9es-des-m%C3%A9thodes-de-pr%C3%A9paration-du-de-Bamba-Dongui/ca62c97384324b34def96ec4abb65bfba33dc14f
11. Bansal, R. C., & Goyal, M. (2005). Activated Carbon Adsorption. CRC Press. https://doi.org/10.1201/9781420028812
12. Basu, S., Ghosh, G., & Saha, S. (2018). Adsorption characteristics of phosphoric acid induced activation of bio-carbon: Equilibrium, kinetics, thermodynamics and batch adsorber design. Process Safety and Environmental Protection, 117, 125–142. https://doi.org/10.1016/j.psep.2018.04.015
13. Boumchita, S, A Lahrichi, Y Benjelloun, S Lairini, V Nenov, et F Zerrouq. 2016. *Elimination d'un colorant cationique dans une solution aqueuse par un déchet alimentaire : Epluchure de pomme de terre [Removal of cationic dye from aqueous solution by a food waste: Potato peel]*.
14. Chyad, T. F., Hammood, Z. A., & Al-Saedi, R. (2025). Agricultural Wastes Derived Activated Carbon for the Removal of Iron from Car-Wash Wastewater. *Ecological Chemistry and Engineering S*, *32*(1), 85-98. https://doi.org/10.2478/eces-2025-0005
15. Coates, J. (2006). Interpretation of Infrared Spectra, A Practical Approach. In R. A. Meyers (Ed.), Encyclopedia of Analytical Chemistry. https://doi.org/10.1002/9780470027318.a5606
16. ASTM Committee D28. (2011). Standard Test Method for Total Ash Content of Activated Carbon. ASTM International. https://doi.org/10.1520/D2866-11
17. Daifullah, A. A. M., Girgis, B. S., & Gad, H. M. H. (2004). A Study of the Factors Affecting the Removal of Humic Acid by Activated Carbon Prepared From Biomass Material. Colloids and Surfaces A: Physicochemical and Engineering Aspects, 235(1-3), 1–10. https://doi.org/10.1016/j.colsurfa.2003.12.020
18. Demiral, I., & Aydın Şamdan, C. (2016). Preparation and Characterisation of Activated Carbon From Pumpkin Seed Shell Using H3PO4. Anadolu University Journal of Science and Technology-A

Applied Sciences and Engineering, 17(1), 125–138. https://doi.org/10.18038/btda.64281
19. Demirbas, A. (2004). Combustion characteristics of different biomass fuels. Progress in Energy and Combustion Science, 30(2), 219-230. https://doi.org/10.1016/j.pecs.2003.10.**004**
20. Foo, K. Y., & Hameed, B. H. (2010). Insights into the modeling of adsorption isotherm systems. Chemical Engineering Journal, 156(1), 2-10. https://doi.org/10.1016/j.cej.2009.09.013.
21. Freundlich, H. (1907). Über die Adsorption in Lösungen. Zeitschrift für Physikalische Chemie, 57U(1), 385-470. https://doi.org/10.1515/zpch-1907-5723
22. Gottipati, R. (2012). Preparation and characterization of microporous activated carbon from biomass and its application in the removal of chromium(VI) from aqueous phase. (PhD thesis). National Institute of Technology, Rourkela. http://ethesis.nitrkl.ac.in/4000/
23. Haghseresht, F., & Lu, G. Q. (1998). Adsorption characteristics of phenolic compounds onto coal-reject-derived adsorbents. Energy & Fuels, 12(6), 1100–1107. https://doi.org/10.1021/ef9801165
24. Han, Q., Wang, J., Goodman, B. A., Xie, J., & Liu, Z. (2020). High Adsorption of Methylene Blue by Activated Carbon Prepared from Phosphoric Acid Treated Eucalyptus Residue. Powder Technology, 366, 239–248. https://doi.org/10.1016/j.powtec.2020.02.013
25. Hashemian, S., Salari, K., & Yazdi, Z. A. (2014). Preparation of activated carbon from agricultural wastes (almond shell and orange peel) for adsorption of 2-pic from aqueous solution. Journal of Industrial and Engineering Chemistry, 20(4), 1892–1900. https://doi.org/10.1016/j.jiec.2013.09.009
26. Ioannidou, O., & Zabaniotou, A. (2007). Agricultural Residues as Precursors for Activated Carbon Production—A Review. Renewable and Sustainable Energy Reviews, 11(9), 1966–2005. https://doi.org/10.1016/j.rser.2006.03.013
27. Jagtoyen, M., & Derbyshire, F. (1998). Activated carbons from yellow poplar and white oak by H3PO4 activation. Carbon, 36(7-8), 1085-1097. https://doi.org/10.1016/S0008-6223(98)00082-7
28. Jawad, A. H., Rashid, R. A., Ishak, M. A. M., & Wilson, L. D. (2016). Adsorption of methylene blue onto activated carbon developed from biomass waste by H2SO4 activation: kinetic, equilibrium and

thermodynamic studies. Desalination and Water Treatment, 57(52), 25194–25206. https://doi.org/10.1080/19443994.2016.1144534

29. Kafando, G. I., Kone, M., Kindo, A., Yamma, R., Sawadogo, J., Tamboura, S., Konate, S., Kutangila, S. M., Zerbo, M., & Bougouma, M. (2025). Groundwater Pollution in Koudougou, Burkina Faso: Chemical and Microbiological Assessment. Asian Journal of Chemical Sciences, 15(1), 16-29. https://doi.org/10.9734/ajocs/2025/v15i1345
30. Khan, M. A., Alqadami, A. A., Wabaidur, S. M., Al-Harbi, M. S., Al-Muhtaseb, A. H., Al-Ghouti, M. A., Otero, M., & Jeon, B. H. (2020). Oil industry waste based non-magnetic and magnetic hydrochar to sequester potentially toxic post-transition metal ions from water. Journal of Hazardous Materials, 400, 123247. https://doi.org/10.1016/j.jhazmat.2020.123247
31. Koné, M., Bonou, L., Bouvet, Y., Joly, P., & Koulidiaty, J. (2009). Study of water pollution by agricultural inputs: Case of five intensive agriculture areas in Burkina Faso. *Sud Sciences & Technologies*, *17*, 6-15. https://www.ajol.info/index.php/sst
32. Kouadio, D. L., Diarra, M., Djassou, A. C., Dibi, B., Dongui, B. K., Mamadou, K., & Traore, K. S. (2022). Experimental study of the adsorption of blue 16 and methyl red on coal from the shell of the cocoa pod. *Journal de la Société Ouest-Africaine de Chimie*, *51*, 17-30. http://www.soachim.org/
33. Kriz Pavia (Author), Lampman (Author). s. d. *Introduction to Spectroscopy*. Thomson Brooks/Cole.
34. Langmuir, I. (1918). THE ADSORPTION OF GASES ON PLANE SURFACES OF GLASS, MICA AND PLATINUM. Journal of the American Chemical Society, 40(9), 1361-1403. https://doi.org/10.1021/ja02242a004
35. Liou, T.-H. (2010). Development of mesoporous structure and high adsorption capacity of biomass-based activated carbon by phosphoric acid and zinc chloride activation. Chemical Engineering Journal, 158(2), 129-142. https://doi.org/10.1016/j.cej.2009.12.016
36. Lopez-Ramon, M. V., Stoeckli, F., Moreno-Castilla, C., & Carrasco-Marin, F. (1999). On the characterization of acidic and basic surface sites on carbons by various techniques. Carbon, 37(8), 1215-1221. https://doi.org/10.1016/S0008-6223(98)00317-0
37. Lua, A. C., & Yang, T. (2004). Effect of activation temperature on the textural and chemical properties of potassium hydroxide activated

carbon prepared from pistachio-nut shell. Journal of Colloid and Interface Science, 274(2), 594-601. https://doi.org/10.1016/j.jcis.2003.10.001

38. Vargas-Rodríguez, Y. M., Obaya, A., García-Petronilo, J. E., Vargas-Rodríguez, G. I., Gómez-Cortés, A., Tavizón, G., & Chávez-Carvayar, J. A. (2021). Adsorption Studies of Aqueous Solutions of Methyl Green for Halloysite Nanotubes: Kinetics, Isotherms, and Thermodynamic Parameters. American Journal of Nanomaterials, 9(1), 1-11. https://doi.org/10.12691/ajn-9-1-1
39. Maazou, S. D. B., Hima, H. I., Malam Alma, M. M., Adamou, Z., & Natatou, I. (2018). Elimination du chrome par du charbon actif élaboré et caractérisé à partir de la coque du noyau de Balanites aegyptiaca. International Journal of Biological and Chemical Sciences, 11(6), 3050-3065. https://doi.org/10.4314/ijbcs.v11i6.39
40. Mandal, S., Stephen, D., & Janardhanan, S. K. (2024). Activated carbon with composite pore structures made from peanut shell and areca nut fibers as sustainable adsorbent material for the efficient removal of active pharmaceuticals from aqueous media. RSC Sustainability, 2(10), 3022-3035. https://doi.org/10.1039/D4SU00262H
41. Melouki, S., Reffas, A., Merrouche, A., Reinert, L., & Duclaux, L. (2020). Biochars derived from common reed for the adsorption of methyl orange in aqueous solution. Revue des Sciences de l'Eau, 32(4), 349-367. https://doi.org/10.7202/1069570ar
42. Mitra, T., Bar, N., & Das, S. K. (2019). Rice Husk: Green Adsorbent for Pb(II) and Cr(VI) Removal from Aqueous Solution—Column Study and GA–NN Modeling. SN Applied Sciences https://doi.org/10.1007/s42452-019-0513-5
43. Mohan, D., & Pittman, C. U., Jr. (2007). Arsenic removal from water/wastewater using adsorbents—A critical review. Journal of Hazardous Materials, 142(1-2), 1–53. https://doi.org/10.1016/j.jhazmat.2007.01.006
44. Molina-Sabio, M., & Rodríguez-Reinoso, F. (2004). Role of Chemical Activation in the Development of Carbon Porosity. Colloids and Surfaces A: Physicochemical and Engineering Aspects, 241(1-3), 15-25. https://doi.org/10.1016/j.colsurfa.2004.04.007
45. Moreno-Castilla, C. (2004). Adsorption of organic molecules from aqueous solutions on carbon materials. Carbon, 42(1), 83-94. https://doi.org/10.1016/j.carbon.2003.09.022

46. Ortiz-Anaya, I., & Nishina, Y. (2024). Refined Surface Area Determination of Graphene Oxide Using Methylene Blue as a Probe Molecule: A Comparative Approach. Bulletin of the Chemical Society of Japan, 97(11), uoae118. https://doi.org/10.1093/bulcsj/uoae118
47. Pan, J., Deng, H., Du, Z., Tian, K., & Zhang, J. (2022). Design of nitrogen-phosphorus-doped biochar and its lead adsorption performance. Environmental Science and Pollution Research, 29(19), 28984–28994. https://doi.org/10.1007/s11356-021-17335-3
48. Patnukao, P., & Pavasant, P. (2008). Activated carbon from Eucalyptus camaldulensis Dehn bark using phosphoric acid activation. Bioresource Technology, 99(17), 8540–8543. https://doi.org/10.1016/j.biortech.2006.10.049
49. Allaire, S. E., & Lange, S. F. (2013). Le biochar dans les milieux poreux : une solution miracle en environnement ?. *Vecteur Environnement*, *46*(4), 58-67. https://www.researchgate.net/publication/308071666_Le_biochar_dans_les_milieux_poreux_Une_solution_miracle_en_environnement
50. Rodríguez Arana, J. M. R., & Reyes Mazzoco, R. (2010). Adsorption studies of methylene blue and phenol onto black stone cherries prepared by chemical activation. Journal of Hazardous Materials, 180(1-3), 656-661. https://doi.org/10.1016/j.jhazmat.2010.04.**086**
51. Sangoremi, A. A. (2025). Preparation and Characterization of Adsorbent Derived from Maize Cob. International Journal of Research and Scientific Innovation, XII(V), 259-269. https://doi.org/10.51244/IJRSI.2025.120500020
52. Socrates, G. 2001. « Infrared and Raman characteristic group frequencies : tables and charts ». https://www.semanticscholar.org/paper/Infrared-and-Raman-characteristic-group-frequencies-Socrates/c13c5a33c987b1483b8ac9a06db0f4f51b7c23f9.
53. Silverstein, R. M., Webster, F. X., & Kiemle, D. J. (2005). Spectrometric identification of organic compounds (7th ed.). John Wiley & Sons. https://www.wiley.com/en-us/Spectrometric+Identification+of+Organic+Compounds,+7th+Edition-p-9780471393623
54. Tchakala, I., Bawa, L. M., Djaneye-Boundjou, G., Doni, K. S., & Nambo, P. (2012). Optimisation du procédé de préparation des charbons actifs par voie chimique (H3PO4) à partir des tourteaux de Karité et des

tourteaux de Coton. International Journal of Biological and Chemical Sciences, 6(1), 461–478. https://doi.org/10.4314/ijbcs.v6i1.42

55. Wabaidur, Saikh Mohammad, Moonis Ali Khan, Masoom Raza Siddiqui, et al. 2020. « Oxygenated Functionalities Enriched MWCNTs Decorated with Silica Coated Spinel Ferrite – A Nanocomposite for Potentially Rapid and Efficient de-Colorization of Aquatic Environment ». *Journal of Molecular Liquids* 317 (novembre): 113916. https://doi.org/10.1016/j.molliq.2020.113916.
56. Wang, Y., Zuo, S., Yang, J., & Yoon, S.-H. (2017). Evolution of Phosphorus-Containing Groups on Activated Carbons during Heat Treatment. Langmuir https://doi.org/10.1021/acs.langmuir.7b00095
57. Yakout, S. M., & Sharaf El-Deen, G. (2011). Characterization of activated carbon prepared by phosphoric acid activation of olive stones. *Arabian Journal of Chemistry*, *9*(novembre), S1155-S1162. https://doi.org/10.1016/j.arabjc.2011.12.002
58. Yap, P. L., Wang, D., & Losic, D. (2025). Advancing Methylene Blue Adsorption Approach for More Precise Measurement of Specific Surface Area of Graphene Oxide. Advanced Materials Interfaces. https://doi.org/10.1002/admi.202500233
59. Yeo, N. A. 2020. *Adsorption des colorants des eaux usées sur du charbon actif et brut issu de la coque d'arachide*. Master de Physique-chimie option Environnement. Université Jean Lorougnon Guédé, République de Côte d'Ivoire.
60. Yorgun, S., & Yıldız, D. (2015). Preparation and characterization of activated carbons from Paulownia wood by chemical activation with H3PO4. Journal of the Taiwan Institute of Chemical Engineers, 53, 122-131. https://doi.org/10.1016/j.jtice.2015.02.032
61. Yuen, F. K., & Hameed, B. H. (2009). Recent developments in the preparation and regeneration of activated carbons by microwaves. Advances in Colloid and Interface Science, 149(1-2), 19-27. https://doi.org/10.1016/j.cis.2008.12.005